Journal of The Electrochemical Society

Outstanding Oxygen Reduction Kinetics of $La_{0.6}Sr_{0.4}FeO_{3-\delta}$ Surfaces Decorated with Platinum Nanoparticles

Journal of The Electrochemical Society, 2020 **167** 104514
1945-7111/2020/167(10)/104514/9/$40.00 © 2020 The Electrochemical Society ("ECS"). Published on behalf of ECS by IOP Publishing Limited

Outstanding Oxygen Reduction Kinetics of $La_{0.6}Sr_{0.4}FeO_{3-\delta}$ Surfaces Decorated with Platinum Nanoparticles

Christoph Riedl,[1,z] Alexander Schmid,[1,*] Andreas Nenning,[1] Harald Summerer,[1] Stefan Smetaczek,[1] Sabine Schwarz,[2] Johannes Bernardi,[2] Alexander Optiz,[1] Andreas Limbeck,[1] and Juergen Fleig[1,,z]**

[1]*Institute of Chemical Technologies and Analytics Technische Universität Wien Getreidemarkt 9 164/EC, 1060 Vienna, Austria*
[2]*Universitäre Service-Einrichtung für Transmissionselektronenmikroskopie (USTEM) Technische Universität Wien Wiedner Hauptstraße 8-10, 1040 Vienna, Austria*

$La_{0.6}Sr_{0.4}FeO_{3-\delta}$ (LSF64) thin films are prepared by pulsed laser deposition (PLD) on yttria stabilized zirconia single crystals (YSZ) and characterized by electrochemical impedance spectroscopy (EIS) measurements before and after decoration with platinum nanoparticles. The platinum on the surface of LSF64 strongly accelerates the oxygen surface exchange kinetics. Especially at low oxygen partial pressures, the area-specific resistance (ASR) decreases by almost two orders of magnitude (e.g. in 0.25 mbar pO_2 from 125 Ωcm^2 to ca. 2 Ωcm^2 at 600 °C). While the pure LSF64 films exhibit severe degradation of the polarization resistance, Pt decorated films degrade much slower and show less scatter between individual samples. Surprisingly, faster oxygen incorporation (=lower polarization resistance) results for lower oxygen partial pressures, which indicates a severe mechanism change compared to undecorated LSF64 surfaces. The obtained results thus also reveal valuable information on the rate-determining step of oxygen exchange on LSF64 surfaces with and without platinum. On undecorated LSF64 surfaces oxygen dissociation is suggested to be rate limiting, while the Pt particles on LSF64 enable fast oxygen dissociation. Consequently, on Pt-decorated LSF64 electrodes a kind of job sharing mechanism results, with oxygen dissociation taking place on Pt and oxide ion formation and incorporation proceeding on the oxide.
 [DOI: 10.1149/1945-7111/ab9c7f]

Manuscript submitted April 21, 2020; revised manuscript received June 2, 2020. Published June 23, 2020.

Supplementary material for this article is available online

Solid oxide fuel cells (SOFCs) directly convert chemical energy of fuels to electric energy at high efficiency and are therefore promising candidates for environmental friendly power generation.[1] Lowering the operation temperature of SOFCs to intermediate temperatures (400 °C–600 °C) is one of the main goals of current research activities and requires new electrode materials, which offer fast oxygen exchange kinetics even at those temperatures.[2–4] Thus, understanding oxygen reduction on the electrode surface is truly essential in order to further improve SOFCs. Perovskite-type mixed ion and electron conductors (MIECs), such as $SrTi_{1-y}Fe_yO_{3-\delta}$ (STF),[5,6] $La_{0.6}Sr_{0.4}FeO_{3-\delta}$ (LSF64),[7–10] $La_{1-x}Sr_xCo_{1-y}Fe_yO_{3-\delta}$ (LSCF),[11,12] $Ba_{1-x}Sr_xCo_{1-y}Fe_yO_{3-\delta}$ (BSCF)[13,14] or $La_{0.6}Sr_{0.4}CoO_{3-\delta}$ (LSC64),[15–20] have been investigated in several studies and are among the most promising candidates for future SOFC electrode materials due to their reasonably high oxygen exchange activity. The oxygen exchange reaction on oxides, written in Kroeger-Vink notation as $\frac{1}{2}O2 + V_O^{\bullet\bullet} + 2e' \leftrightarrow O_O^{\times}$ was already investigated in numerous other studies, see e.g.[18,21–37] Besides fast oxygen reduction kinetics, future SOFC electrodes should also offer morphological stability, possess high ionic and electronic conductivity, be compatibile with other materials of the cell[38] and show little degradation.[39]

For operating SOFCs, porous electrodes are used due to their large surface area for oxygen reduction. However, in fundamental research often dense MIEC thin films, prepared by pulsed laser deposition (PLD), are employed in order to obtain model-type electrodes with well-defined geometry. On these dense MIEC thin film electrodes, the oxygen reduction reaction takes place via the so-called bulk-path, which involves oxygen gas diffusion, adsorption of O_2 on the electrode surface, dissociation, ionization, and incorporation into the oxide.[21] Understanding all individual reaction steps, identifying the rate determining step and finding ways to accelerate this step will contribute to the development and improvement of new cathode materials for SOFCs. For example, on $La_{0.6}Sr_{0.4}CoO_{3-\delta}$ (LSC64) already tiny amounts of SrO cause a severe decrease of the cathode performance and small amounts of Co lead to (re)-activation of the cathode.[16] These results also indicate that the rates of the oxygen reduction reaction may strongly depend on the catalytic effect of a few highly active sites on the MIEC surface.

Platinum is known for its catalytic properties especially in aqueous systems and in polymer electrolyte membrane fuel cells (PEM-FC), which operate below 100 °C. In these cells, platinum nanoparticles (pure or alloyed) are used to accelaterate the oxygen reduction reaction (ORR) at the cathode[40] and much research has been done to understand the ORR, to improve its performance,[41] to understand the size effect of platinum particles on the ORR[42] or to develop non-platinum catalysts.[43] However, the exact intermediate steps of the ORR mechanism are still debated, also because of difficulties in detecting the intermediate species of the ORR.[44] In the field of ceramic oxide ion conductors, porous Pt electrodes are commonly used in oxygen sensors[45] and also many fundamental studies have been performed to understand oxygen reduction, for example at Pt|YSZ interfaces.[37,46–59]

Interestingly, Pt electrodes are very rarely used in SOFCs, not only because of costs but also because Pt electrodes generally lead to higher polarization resistances than cathodes made of mixed conducting oxides. This may be surprising since Pt is known to catalyze dissociation of oxygen molecules.[60,61] However, in YSZ|Pt cathodes for SOFCs the oxygen reduction reaction is limited to the so-called triple phase boundary (TPB),[46] in contrast to the entire surface being potentially active in case of a MIEC cathode.[62] Accordingly, the number of electrochemically active sites is rather small, compared to mixed conducting electrode materials. This raises the question whether changes in the electrode design may help still exploiting the oxygen splitting capability of platinum.

Several studies have been conducted adressing the effect of surface decoration on the ORR kinetics of MIEC electrodes, but unfortunately reports often show very contradictory results. For example, while Uchida et al. showed that nanometer-sized Pt or Pt-Rh catalysts on LSM particles greatly reduced the cathodic overpotential[63] and Erning et al. reported similar effects with Pd

*Electrochemical Society Student Member.
**Electrochemical Society Fellow.
[z]E-mail: christoph.riedl@tuwien.ac.at; juergen.fleig@tuwien.ac.at

particles on LSM,[64] Haanappel et al. did not measure any positve electrocatalytic effects of Pt on LSM.[65] In a recent study by Piage et al. it was shown that dopant levels of Co and Ni on the surface of LSF-YSZ improved the electrochemical performance, while PdO did not lower the polarization resistance.[66] Moreover, a study by Cheng et al. revealed that submonolayer amounts of Ca, Sr, Pr or La lowered the polarization resistance of porous LSF-YSZ composite electrodes.[67] In another study conducted on LSF and LSM it was assumed that different dopants rather improve the electrode performance by a structural change of the electrode surface than by improved catalytic properties.[68]

In the studies mentioned above measurements were all conducted on porous MIEC electrodes and the electrochemical performance was exclusively studied in (synthetic) air. In this study, we used platinum nanoparticles to accelerate the oxygen reduction on $La_{0.6}Sr_{0.4}FeO_{3-\delta}$ (LSF64) thin films and measured the performance improvement of the electrode by electrochemical impedance spectroscopy at different oxygen partial pressures. Symmetrical thin film electrodes were prepared by pulsed laser deposition of LSF64 on yttria stabilized zirconia single crystals (YSZ) and investigated before and after sputter deposition of tiny amounts of Pt (nominally a few monolayers) onto the LSF64 surface. We show that a huge performance improvement is possible, especially in reduced oxygen partial pressure (only ca. 2 Ωcm^2 polarization resistance at 600 °C in 0.25 mbar pO_2). Moreover, from the partial pressure dependence, degradation behavior and reproducibility studies we can draw far-reaching conclusions on the oxygen reduction mechanism of these surface decorated MIEC electrodes.

Experimental

Platinum current collector grids with either 25/10 μm mesh/strip width or 10/10 μm mesh/strip width were prepared on both sides of YSZ(100) single crystals ($0.5 * 0.5 * 0.05\ cm^3$) (CrysTec, Germany) by lift-off lithography and subsequent magnetron sputter deposition of 5 nm titanum and 100 nm platinum. Dense $La_{0.6}Sr_{0.4}FeO_{3-\delta}$ (LSF64) thin films were prepared on top of those current collectors by pulsed laser deposition (PLD). LSF64 powder was synthesized via the Pechini route from Fe, La_2O_3 and $SrCO_3$ and the PLD target was then prepared by isostatic pressing (150 MPa) and sintering at 1200 °C for 12 h. Laser ablation was performed at 600 °C substrate temperature and 0.04 mbar oxygen partial pressure (Alphagaz™, 99.995%) with a KrF excimer laser (Complex Pro 210F, wavelength 248 nm) at a frequency of 5 Hz, a laser energy of 2 J cm^{-2} and a target to substrate distance of 6 cm. The deposition time was 30 min (9000 pulses) leading to a LSF64 thickness of 200 nm. The resulting samples are sketched in Fig. 1a.

For impedance measurements, samples were contacted with platinum meshes (75/500 μm strip/width) and heated to 600 °C in a measurement station made of Al_2O_3 (corundum). Electrochemical Impedance Spectroscopy (EIS) measurements were done with a Novocontrol Alpha Frequency Analyzer (Novocontrol Technologies, Germany) from 10^6 to 10^{-2} Hz and an AC amplitude of 10 mV. The integration time was either 1 s or 1 period. Oxygen partial pressures between 210 mbar and 0.25 mbar were investigated.

After initial electrochemical characterization of the pristine samples, samples were held upon measurement conditions for several hours to observe degradation. After cooling samples down to room temperature, the surface of the thin films was decorated with platinum particles. This was done by magnetron sputter deposition (BAL-TEC MED 020, Liechtenstein) for a very short time at a pressure of $2 * 10^{-2}$ mbar Ar and a sputter current of 100 mA. The typical deposition time was 2 s. However, to vary the Pt amount, the sputter current (between 25 and 100 mA) and the sputter duration (between 2 and 5 s) was also varied. For the standard conditions (2 s, 100 mA) a Pt layer with a nominal thickness of 1.6 nm is obtained. However, at measurement temperatures this layer agglomerates to small Pt nanoparticles, see sketch in Fig. 1a and section Results. The obtained symmetrical samples with Pt decorated LSF64 electrodes were then again electrochemically characterized by means of impedance spectrocopy.

In order to investigate the deposited amount of platinum, additional YSZ(100) single crystals were positioned in the sputter chamber next to the YSZ samples with LSF64. Afterwards the platinum was dissolved from the YSZ with concentrated aqua regia ($HCl:HNO_3 = 3:1$) and the solution was diluted with distilled water. Chemical analysis was performed with an inductively coupled plasma mass spectrometry (ICP-MS) iCAP Q (Thermo Scientific, United States of America). Scanning electron microscopy (SEM) measurements were carried out with a FEI Quanta 250 FEGSEM. The morphology was determined by analyzing secondary electrons images (SE) and backscattered electrons images (BSE). Samples for transmission electron microscopy (TEM) were prepared with a Quanta 200 3D DualBeam-FIB and measured with a FEI TECNAI F20. Grazing incidence measurements were performed with a Empyrean X-ray diffractometer (Malvern Panalytical) equipped with a parallel beam mirror on the incident beam side and a parallel plate collimator and a scintillation detector on the diffracted beam side. Measurements in Bragg-Bretano geometry were performed with an Malvern Panalytical, MPD Pro.

Results

Morphological, structural and chemical characterization.—To characterize the surface composition and morphology of the Pt

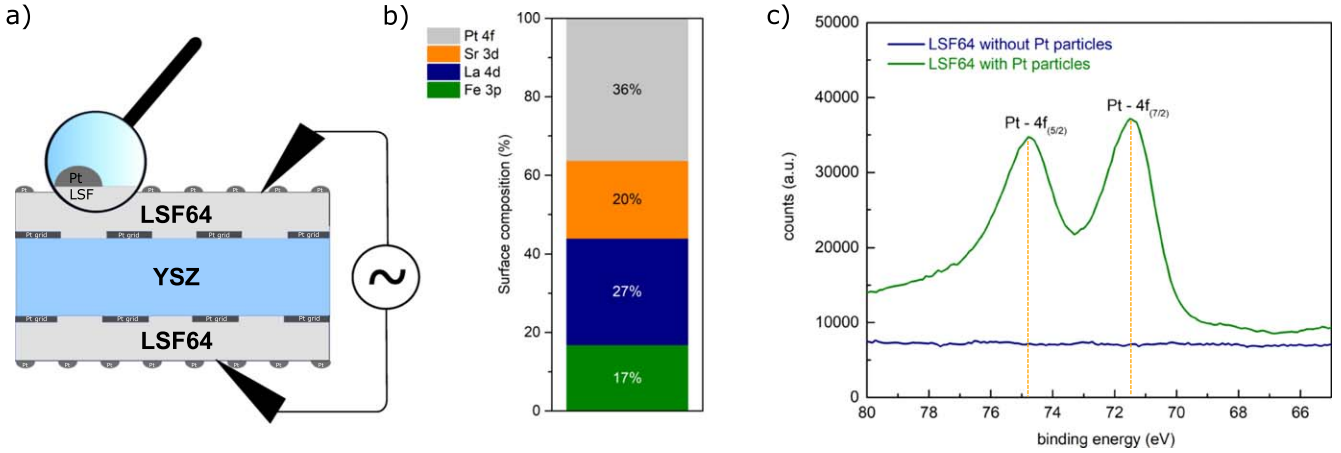

Figure 1. (a) Sample sketch with embedded current collecting Pt grid at the LSF64|YSZ interface and catalytically active Pt nanoparticles on top of LSF64. (b) Surface composition of a platinum decorated LSF64 electrode analyzed from XPS spectra measured after heating to 600 °C for 14 h. (c) Section of the XPS spectra showing a pristine LSF64 electrode and a LSF64 electrode decorated with platinum nanoparticles.

decorated LSF64 thin film electrodes, several analytical techniques were applied. The amount of platinum on the electrodes was quantified by ICP-MS measurements. The applied standard procedure of Pt deposition (0.854 ± 0.034 μg on 0.25 cm^2) corresponds to a film thickness of 1.6 nm assuming a continuous layer. However, after heating to 600 °C in the measurement setup, surface morphology characterization revealed agglomerated Pt particles in accordance with literature.[69] SEM in BSE mode clearly shows the difference between a pristine LSF64 (Fig. 2d) and a platinum decorated LSF64 electrode Fig. 2e. According to SEM images, the size of the platinum particles was between 20 nm and 40 nm. This was also confirmed by transmission electron microscopy (TEM) measurements, see (Figs. 2a–2c). The platinum particles had an average height of about 6 nm in the TEM images. Comparision with the nominal thickness of 1.6 nm this indicates a surface coverage in the range of 30%.

This is also in good accordance with X-ray photoelectron spectroscopy (XPS) measurements. Those revealed a surface composition with about 36% of the surface atoms being platinum see Fig. 1b. Moreover, XPS measurements showed that the oxidation state of platinum was Pt(0) and no evidence was found that platinum had oxidized to PtO or PtO_2 during electrochemical measurements (Fig. 1c). The binding energy found for the Pt-$4f_{(5/2)}$[70] and the Pt-$4f_{(7/2)}$[71] line corresponds to metallic Pt. The crystallinity of the LSF64 films is clearly shown in the diffractograms (see Supporting Information Fig. S1 available online at stacks.iop.org/JES/167/104514/mmedia). The polycrystalline columnar nature of the LSF64 film growth is also visible in the TEM images. Owing to their small amount and size, it was not possible to detect any signal from the platinum particles on the surface of LSF64 by means of the lab-based diffractometer.

The effect of platinum nanoparticles on the oxygen exchange reaction at the LSF64 surface—impedance spectra.—The electrochemical properties of the LSF64 electrode were investigated on samples with symmetrical LSF64 electrodes, as sketched in Fig. 1a. The strong electrochemical effect of platinum nanoparticles on the surface of LSF64 is displayed in the impedance spectra of Figs. 3a–3c, measured on three different samples in different gas atmospheres (0.25 mbar, 10 mbar, 210 mbar O_2). The plots show the spectra obtained on pristine LSF64, spectra measured after some time at elevated temperature under measurement conditions (degradation) and spectra obtained on the same samples after Pt particle deposition. The degradation of the electrochemical performance for pristine LSF surfaces is a well-known phenomenon and mostly attributed to Sr segregation.[17,72–74] Also the XPS measurements in this study show a significant surface enrichment of A-site cations (see below).

The impedance spectra were fitted using the equivalent circuits shown as insets in Fig. 3. All spectra exhibit a high-frequency intercept, which did not show any oxygen partial pressure dependency and can be assigned to transport of O^{2-} ions through the YSZ single crystal.[11] Small differences of the high-frequency intercept can be explained by slightly different temperatures of the samples. The dominating semicircle in the low frequency range displays a strong dependency on the oxygen partial pressure and can be assigned to the oxygen exchange reaction on the electrode surface.[11,13,75] This semicircle was fitted to an R|CPE element (CPE = constant phase element). In the medium frequency range often a slight shoulder of the main arc is found, which can most likely be attributed to the LSF64|YSZ interface. However, this rather small part was neglected in most fits. In the following, we label the surface related resistance of the main arc R_{pol}. The electrode capacitance, modeled by the constant phase element (CPE) is attributed to the chemical capacitance and thus to oxygen stoichiometry changes in the bulk of the electrode.[76]

Area specific resistances (ASR) of the individual electrodes were calculated from the polarization resistances R_{pol} and the active area and are plotted in Fig. 3d. Earlier measurements showed that only the area of LSF64 films directly above YSZ contributes to the oxygen exchange reaction, while the LSF64 above the current collecting Pt grid is inactive due to the relatively large in-plane ionic resistance in the films.[8] Hence, the active surface area used in this analysis was only 25% or 50% of the total area depending on the platinum current collector used. However, the area covered by the Pt nanoparticles was not included in this normalisation. As can be seen from Fig. 3, the deposition of platinum nanoparticles always led to a strong decrease of the area-specific resistance. The effect of the platinum nanoparticles was especially prounounced at low oxygen partial pressures (0.25 mbar), where the pristine sample exhibited rather slow kinetics. The improvement of Pt with respect to the initial value (LSF64 as deposited) was a factor of 70 and compared to the degraded state of the free LSF64 surface the Pt particles lead to >200 times better kinetics. Interestingly, also the degradation of

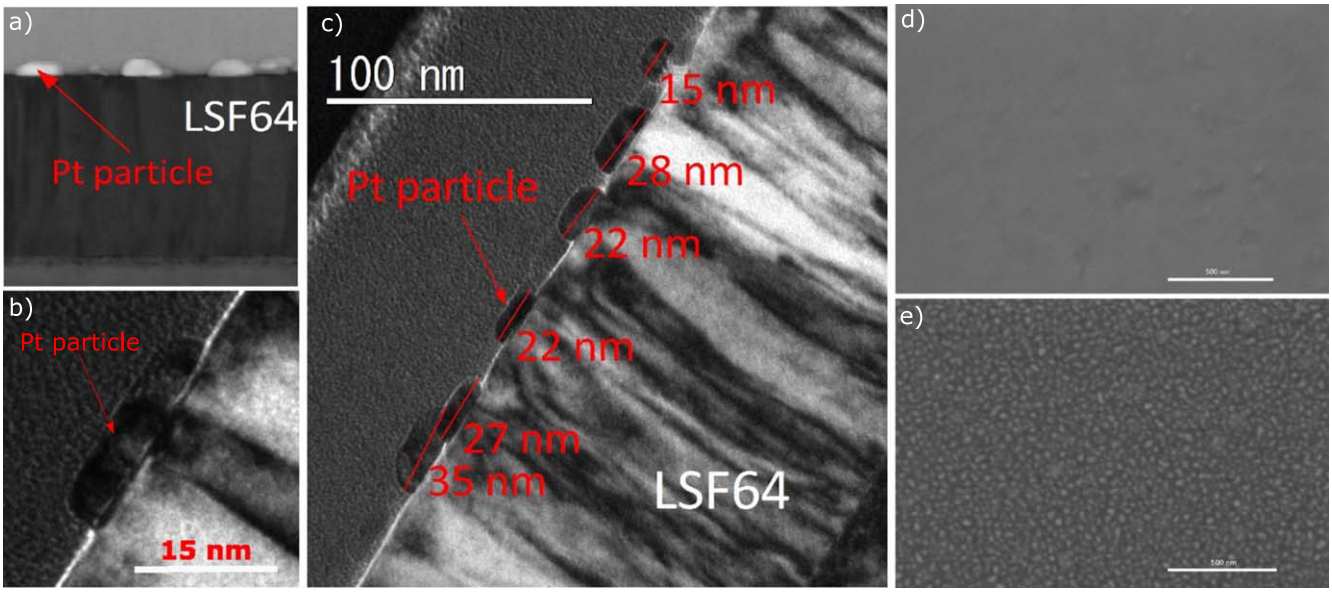

Figure 2. (a) STEM image of a platinum decorated LSF64 electrode. (b) magnified TEM image of a single platinum nanoparticle on LSF64. (c) FIB-TEM image of a platinum decorated LSF64 electrode. (d) SEM image of pristine LSF64 electrode. (e) SEM image of a platinum decorated LSF64 electrode after 16 h in 0.25 mbar O_2 at 600 °C.

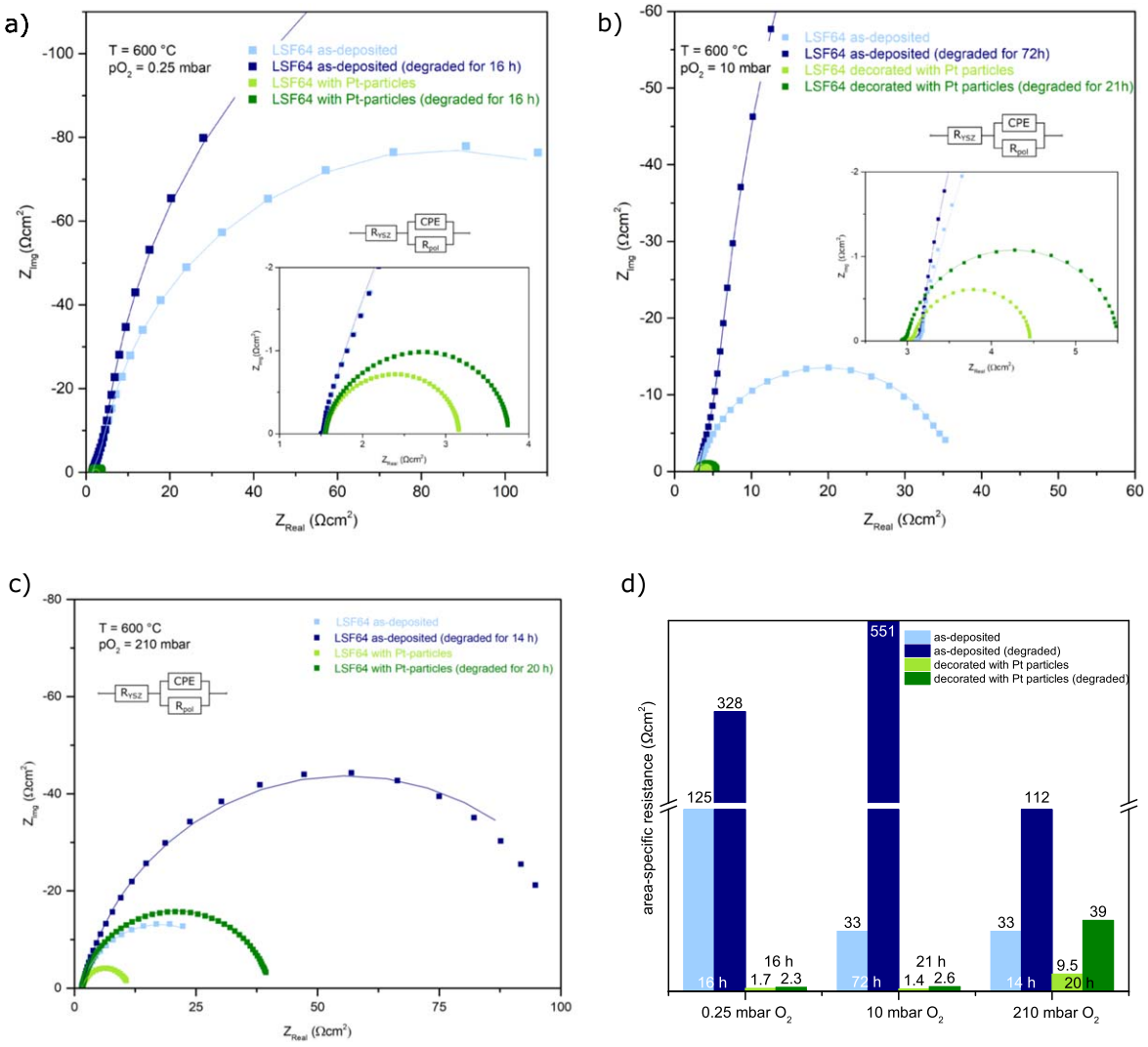

Figure 3. (a)–(c) Impedance spectra of symmetrical samples with LSF64 electrodes measured at 600 °C in 0.25 mbar O_2 (a), 10 mbar O_2 (b) and 210 mbar O_2 (c) before and after platinum decoration. The impedance data are normalized to the active electrode area and divided by two (to reveal ASR values of one electrode). Symbols are measured data, lines are fits to the equivalent circuits shown in the insets. (d) Bar chart showing the area specific resistance of LSF64 electrodes at 600 °C before and after platinum decoration. Times written on the bars indicate degradation times. For all samples the standard Pt amount of 0.854 μg on 0.25 cm^2 was used.

the electrode was much less pronounced with the Pt particles. In synthetic air (210 mbar O_2) Pt improved the reaction rate less (still a factor >3) and degradation with Pt particles was also faster.

The chemical capacitance (C_{chem}) of the electrodes was calculated from the obtained fitting parameters of the CPE element according to $C_{chem} = (Q * R_{pol}^{1-n})^{\frac{1}{n}}$, with Q and n being the fit parameters of the CPE element.[77] The values measured without Pt are in reasonable agreement with literature.[7] However, a strong decrease of the capacitance is found after the platinum deposition, as can be seen from Table I. The change of the capacitance is most pronounced for measurements at 0.25 mbar O_2, with a decrease by a factor of about 2. A fitting artefact was excluded to be the reason behind the change of the chemical capacitance, because the exponent n of the CPE remained the same for the decorated and the undecorated sample (≈0.9). According to literature the chemical capacitance of a mixed conducting thin film can be attributed to oxygen stoichiometry changes in the bulk of the electrode.[78] Then, however, the Pt surface decoration is not expected to change the corresponding bulk related values, which should be proportional to the sampled volume.[7] The active MIEC electrode volume should not change due to decoration. So far, we do not have a simple explaination for the process behind the decrease of the chemical capacitance after platinum decoration. Since the focus of the present work is laid on the effect of Pt decoration on the surface exchange

Table I. Chemical capacitance at 600 °C measured in different gases with and without Pt decoration. Standard Pt amount, i.e. 0.854 ± 0.034 on 0.25 cm^2.

gas	before Pt decoration	after Pt decoration	literature value[7]
0.25 mbar pO_2	3700 F cm^{-3}	1500 F cm^{-3}	3300 F cm^{-3}
10 mbar pO_2	1470 F cm^{-3}	860 F cm^{-3}	1600 F cm^{-3}
210 mbar pO_2	1300 F cm^{-3}	1000 F cm^{-3}	750 F cm^{-3}

reaction, a detailed discussion of this effect on C_{chem} is beyond the scope of this paper and will be the topic of future studies.

Oxygen partial pressure dependency of the polarization resistance.—Platinum decorated LSF64 electrodes were measured in different oxygen partial pressures (210 mbar to 0.25 mbar) at 600 °C. As can be seen from the spectra in Fig. 4a, a rather unusual strong increase of the reaction rate—i.e. decrease of the polarization resistance- is found for lower oxygen partial pressures. Kinetic studies on mixed conducting oxides usually show faster oxygen incorporation at higher oxygen partial pressure,[7,15,19,79–83] in accordance with standard expectations for kinetic models of oxygen reduction (more oxygen molecules enhance the reaction rate). The surprising pO_2 dependence of the ASR was analyzed in terms of a power law with an exponent m according to $ASR^{-1} = \alpha * p_{O_2}{}^{m}$, i.e. $-\log(ASR) = \log(\alpha) + m * \log(p_{O_2})$. In Fig. 4b the negative logarithm of the ASR is plotted against the logarithm of the pO_2 and a reaction order n of −0.41 is found.

The negative reaction order is completely opposite of what is found for LSF64 surfaces without Pt, where a reaction order of +0.73 was measured between 0.25 and 50 mbar as reported in literature[84] for nominally identical LSF64 electrodes (see also Fig. 4b. Obviously, deposition of Pt particles leads to a situation, where an increase of the oxygen concentration in the gas phase does not enhance the reaction rate of oxygen reduction, but rather decreases it. Interestingly, the obtained reaction order is rather close to the slope (−0.5) of the concentration of oxygen vacancies $V_O^{\bullet\bullet}$ in the high pressure range of the Brouwer diagram[7,85] of LSF64, suggesting a correlation of reaction kinetics and defect concentration. The proposed reaction mechanism is further discussed below. Please note that in Fig. 4b two different samples were considered, one with Pt and one without Pt. In Fig. 3, on the other hand, one and the same sample was used for investigating the effect of Pt decoration in a given atmosphere, while different samples were used in different gases. Owing to the scatter of values from sample to sample, see also below, absolute values may thus differ despite nominally identical PLD preparation conditions. Most relevant in Fig. 4b are the very different reaction orders with and without Pt.

Effect of the deposited platinum amount on the polarization resistance.—In an additional experiment the deposited amount of platinum was varied. The LSF64 films were prepared in one single batch in the PLD and measured at 600 °C and 10 mbar O_2 partial pressure before and after platinum decoration. In Fig. 5 the impedance spectra after Pt deposition are displayed and the area specific resistances of all samples are summarized. As can be seen from the impedance spectra, the deposited platinum amount has a clear effect on the area specific resistance of the LSF64 electrodes and the lowest polarization resistance is found for 0.383 μg Pt on 0.25 cm^2. Similar to earlier studies[8,78] the polarization resistance of pristine LSF scatters strongly, but the initial value does not show any correlation with the value found after Pt decoration.

XPS was carried out to investigate the surface composition of each sample and thus the surface coverage with Pt. The deposited Pt amount was obtained by ICP-MS. As can be seen from the results in Fig. 5, the surface coverage with platinum does not increase linearly with the deposited platinum amount. This is most probably due to a change of the Pt particle height. Assuming cylindrically shaped particles, the average height of the platinum particles was calculated from the results in Fig. 5 and the resulting values (between about 3 and 8 nm) are summarized in Table II. BSE images of every sample surface can be found in the Supporting Information (Fig. S2).

The measured polarization resistance results suggest that there is an optimum amount of platinum on the surface of LSF64. An increase of the deposited platinum amount beyond this value leads to increased area specific resistances. Not surprisingly, also too little Pt is disadvantageous. However, it is though remarkable that already the deposition of 0.171 μg platinum on 0.25 cm^2 (surface coverage 9% Pt) led to an improvement of the area specific resistance from 65 Ωcm^2 to 15 Ωcm^2 at 10 mbar O_2.

Effect of sample prehistory and degradation on the resistance of platinum decorated electrodes.—Also the effect of sample prehistory and sample degradation on the area specific resistance of platinum decorated electrodes was further investigated. Four samples with symmetrical LSF64 electrodes (A-D) were prepared in one batch in the PLD chamber and were also sputter-coated with Pt in one batch to exclude effects of varying platinum amounts. Impedance measurements were carried out at 600 °C and 10 mbar O_2 partial pressure. While sample A and sample B were measured for 19 h and 72 h respectively, sample C and sample D were not exposed to measurement conditions before platinum deposition. In Table III the measured polarization resistances are summarized and reveal that the sample prehistory or degradation does not have a significant influence on the observed resistance values of the platinum decorated electrodes.

All four platinum decorated samples showed very similar area specific resistances between 1.1 Ωcm^2–1.4 Ωcm^2 and fairly comparable and moderate degradation behavior. Pt free samples A,B, on the other hand had very different polarization resistances and degradation behavior, in agreement with the results and data scattering presented above and mentioned in literature for perovskite type thin film electrodes.[8] While sample A showed very fast oxygen reduction kinetics with an area specific resistance of 9.5 Ωcm^2 and degraded

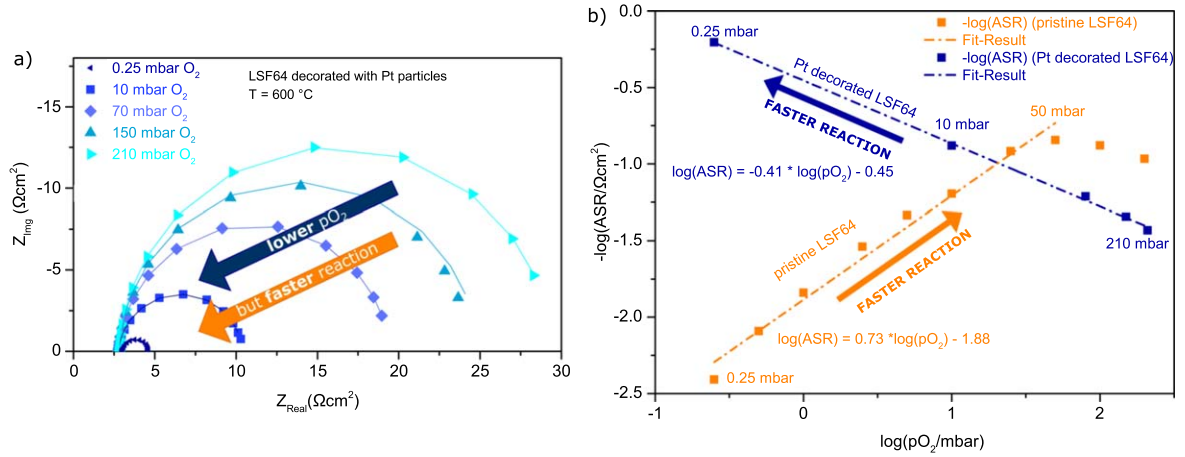

Figure 4. (a) Impedance spectra of a sample with LSF64 electrodes decorated with Pt particles, measured at different pO_2, revealing faster oxygen incorporation at lower pO_2. (b) ASR vs pO_2 on a −log/log-scale for a pristine sample with LSF64 electrodes (orange data points) from reference[84] and a sample with platinum decorated LSF64 electrodes (blue data points)standard Pt amount, i.e. 0.854 μg on 0.25 cm^2, all measured at 600 °C.

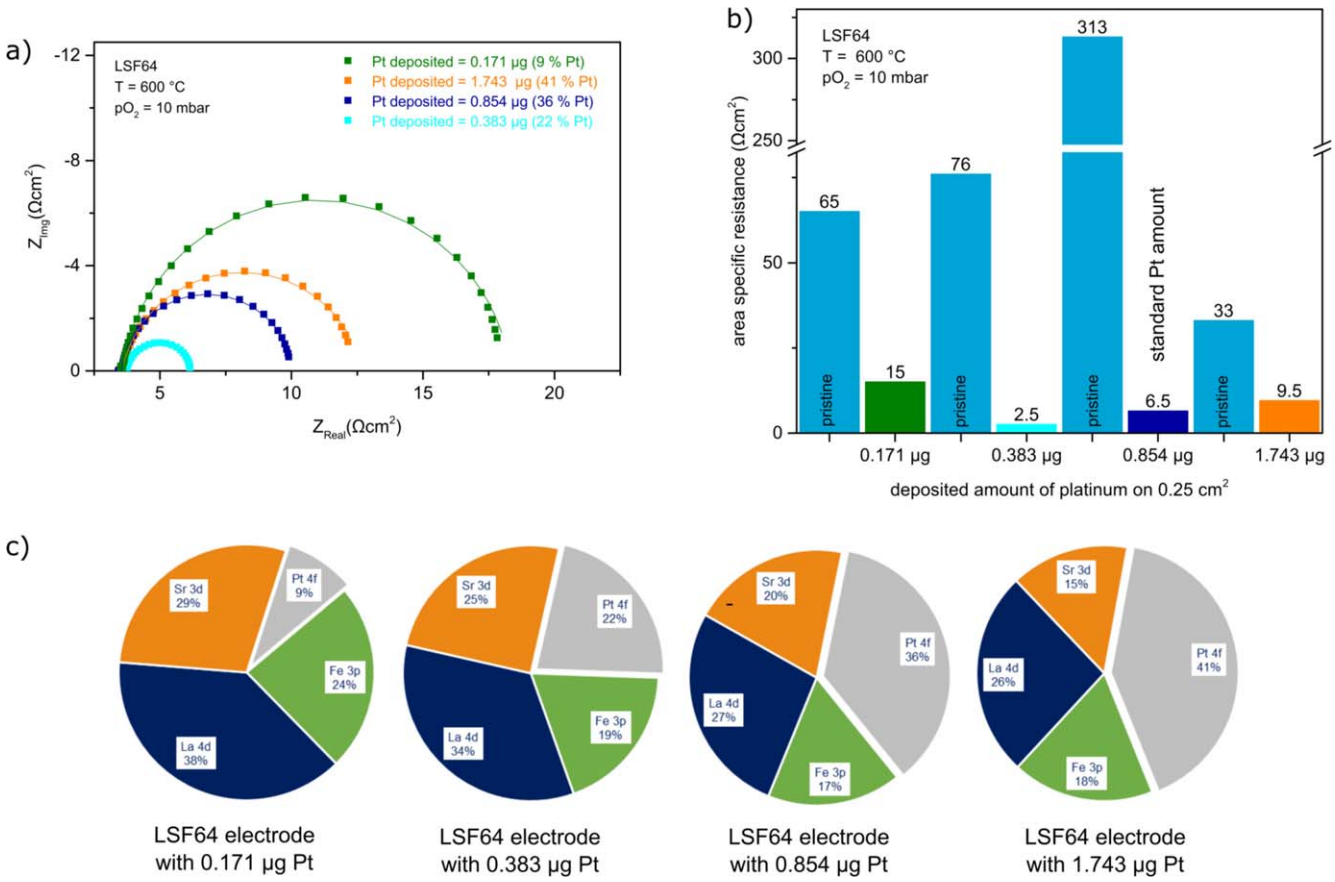

Figure 5. (a) Impedance spectra of four different LSF64 electrodes decorated with different amounts of platinum and measured at 600 °C in 10 mbar pO_2. (b) Bar chart summarizing the effect of different amounts of platinum on the polarization resistance of LSF64 electrodes. (c) Surface composition of all investigated samples from (a) measured by XPS.

Table II. Height of the platinum particles calculated from the deposited amount of Pt on 0.25 cm² (from ICP-MS) and the estimated surface coverage (from XPS).

	deposited Pt (μg)	**surface Pt** (%)	**particle height** (nm)
Sample 1	0.171 ± 0.008	9	3
Sample 2	0.383 ± 0.004	22	3
Sample 3	0.854 ± 0.034	36	4
Sample 4	1.743 ± 0.069	41	8

Table III. Effect of degradation and sample prehistory of four identically prepared samples with LSF64 electrodes (A-D) (one batch) with and without platinum decoration. Standard Pt amount of 0.854 ± 0.004 on 0.25 cm². "Time" indicates degradation time.

	pristine LSF64 samples			**platinum decorated LSF64 samples**		
	as-deposited	degraded	time	as-deposited	degraded	time
A	9.5 Ωcm²	14.5 Ωcm²	19 h	1.2 Ωcm²	2.6 Ωcm²	21 h
B	33 Ωcm²	551 Ωcm²	72 h	1.4 Ωcm²	2.6 Ωcm²	21 h
C		not measured		1.1 Ωcm²	1.8 Ωcm²	23 h
D		not measured		1.2 Ωcm²	2.1 Ωcm²	23 h

very slowly to 14.5 Ωcm² in 19 h, sample B exhibited much worse oxygen reduction kinetics already in the pristine state with an area specific resistance of 33 Ωcm², which degraded quickly to about 551 Ωcm² after 72 h of measurement. The very similar ASR values found after Pt deposition show that the Pt particles obviously affect the oxygen exchange reaction in a manner neither depending on the intial state of the LSF64 surface nor on its degraded state. This is another very strong indication that a severe change of the reaction mechanism or the rate limiting step takes place with Pt on the surface. As a result of this mechanistic modification, the polarization resistance becomes much less prone to changes of the MIEC surface. In the Supporting Information it is shown that such an effect of Pt nanoparticles is not restricted to LSF64, but can also be found for $SrTi_{0.7}Fe_{0.3}O_{3-\delta}$ (STF73). Moreover, the Pt nanoparticles also improve the polarization resistance of LSF64 in humidified hydrogen.

Mechanistic Discussion

The results shown so far have strong implications for the mechanistic interpretation of oxygen exchange on mixed conducting oxides, here LSF64. Essentially five experimental facts have to be explained:

(i) the strong reduction of the polarization resistance by Pt decoration, especially at low oxygen partial pressures (0.25 mbar O_2)
(ii) the surprising negative reaction order, i.e. the much faster reaction upon lower pO_2.
(iii) the increase of the polarization resistance for very small amounts of platinum (0.171 μg Pt, 9% surface coverage (XPS)).
(iv) the high reproducibility of the polarization resistance with Pt decoration, irrespective of the LSF64 degradation state.
(v) the reduced degradation rate with Pt.

In the following we suggest a simple mechanistic model that can explain all these effects. We base our discussion on the reaction mechanism for oxygen incorporation on single phase MIEC cathodes proposed in Ref. 21: On dense thin film samples, oxygen reduction and incorporation takes place via the so-called bulk path. In this path oxygen gas diffuses to the electrode, adsorbs on the surface of the oxide, dissociates and is incorporated into an oxygen vacancy. The ionization steps may take place during dissociation and/or during incorporation. The oxygen ions are then transfered through the electrode to the electrolyte. Electrons needed for the oxygen reduction are transported from the current collector to the active reduction site on the surface of the MIEC oxide. This is sketched in Fig. 6, together with the modification that comes along with the Pt particles.

With Pt on the MIEC surface, oxygen (O_2) from the gas phase adsorbs on the Pt surface and dissociates. The resulting oxygen (O_{ad}) atom (possibly partly charged) then diffuses from the platinum particle onto the free, uncovered MIEC electrode surface (=spill-over) and gets incorporated into the oxide. The final ionisation step may take place either before or during incorporation into the oxide lattice. In contrast to standard triple-phase boundary electrodes, the oxygen vacancy and also the electrons required for oxygen incorporation are provided by the mixed conductor. For a steady state reaction, the electrons flow from the current collector into the MIEC, while oxygen vacancies are replaced from the electrolyte.

The decreased polarization resistance of platinum decorated MIEC samples (observation i)), can then easily be explained by a complete change of the rate limiting step, induced by the presence of Pt. Since Pt can only accelerate the oxygen dissociation, but not the incorporation into a MIEC oxygen vacancy, we conclude that oxygen reduction on free MIEC surfaces is most probably limited by oxygen dissociation (possibly including partial ionization). This rate limiting dissociation step is now bypassed by the platinum particles. Hence, we have a kind of job splitting between platinum particles (oxygen dissociation) and MIEC oxygen incorporation. This is a true two phase process and not an effect of the MIEC|Pt interface.

Consequently, the geometric dependencies of R_{pol} may become rather complicated, since at least three geometrical parameters may play a role: first, the surface area of Pt (required for oxygen dissociation), second the surface area of LSF64 (required for ionization and incorporation) and third the distance between two Pt particles or between two triple phase boundaries (affecting the required spill-over distance). A complete mechanistic model thus requires extensive parameter variation and morphological characterization. However, in the following we show that already from the existing data important mechanistic conclusions can be drawn.

Since less platinum surface area and thus more free MIEC surface can still lower the resistance (observation iii)), we conclude that also with platinum particles on top, the rate limiting step takes

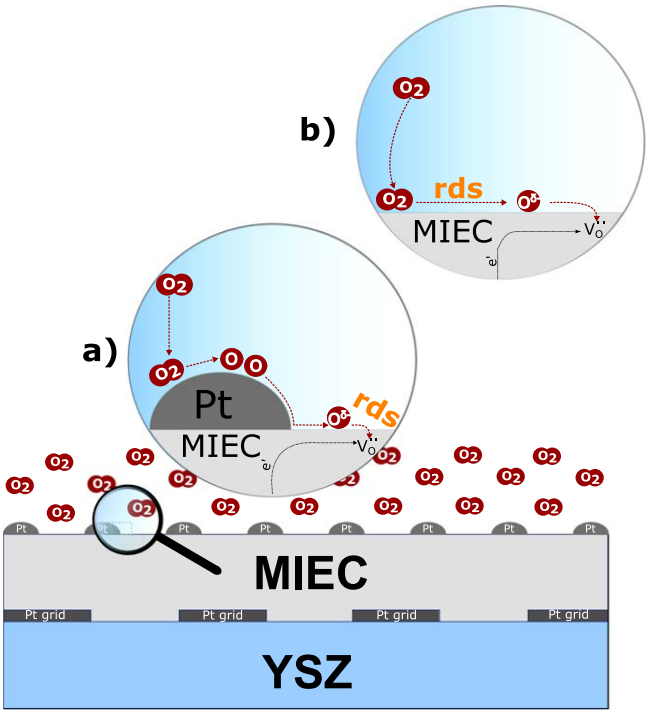

Figure 6. Sketch explaining the suggested reaction mechanism for oxygen incorporation on a platinum decorated MIEC (a) and a pristine MIEC (b).

place on the MIEC surface. A rate limiting step on Pt should show the opposite trend. Oxygen adsorption and dissociation on the platinum particles thus seems to be sufficiently fast, even for very low pO_2, at least compared to LSF.[86–88] Hence, no longer oxygen dissociation on the MIEC is decisive, but oxygen incorporation into the MIEC (i.e. into a vacancy) and/or ionization. This change of the rate limiting step also explains the surprising pO_2 dependence (observation ii)): At higher oxygen partial pressures the concentration of O_2 in the gas atmosphere is higher and this accelerates the rate limiting dissocation on free LSF64 in accordance with the measurements. With Pt, oxygen incorporation into an oxygen vacancy on the MIEC becomes the decisive step. According to the Brouwer diagram of LSF64[84] the concentration of oxygen vacancies is higher at lower pO_2 and therefore the incorporation of oxygen is faster at lower oxygen partial pressures. Since both, empirical reaction order of ASR^{-1} vs pO_2 (−0.41) and slope in the Brouwer diagram (−0.5) are very similar, the true reaction order with respect to the oxygen vacancies seems to be close to 1.[7,84,85]

According to this reaction scheme the rate limiting dissocation step on pure MIEC materials (here LSF64) depends very strongly on active sites for dissociation. Those maybe severely affected by prehistory and degradation. Moreover, the number of very active dissociation sites appears to be strongly limited anyway: A study on LSC showed that already a few percent of a SrO monolayer double the polarization resistance and can deactivate most of the highly active sites on LSC.[16] All this may cause the strong scatter of polarization resistance often found on pure MIEC electrodes.The rate limiting oxygen incorporation for platinum decorated MIECs, however, is related to the oxygen vacancy concentration, which seems to be less prone to changes or deactivation. This would explain observations v) and vi) i.e. the high reproducibility and the reasonable stability of the polarization resistance for the Pt decorated LSF64.

Lowering the platinum amount to 9% surface coverage (observation iv)) led to an increase of the area-specific resistance. The observation can be explained if one assumes that the spill-over of atomic oxygen onto LSF64 surfaces is limited to a distinct zone close to the TPB. This would imply that the area supplied with

dissociated oxygen species and thus being active for oxygen incorporation (i.e. rings around the Pt particles) becomes smaller than the entire free MIEC surface very few and distant Pt particles. Then a co-limitation of oxygen surface diffusion on the MIEC and oxygen incorporation (into a vacancy) becomes effective. This interpretation is also supported by several earlier studies,[5,8] where Pt current collector grids were deposited on top of the MIEC thin film surfaces, but the strong catalytic effect of platinum (especially the negative pO_2 dependence of the area specific resistance) has not been observed. Most probably this is also a geometrical effect: While Pt current collector width and distances are in the range of several micrometers, the deposited platinum nanoparticles in this study were in the range of 20–40 nm. The limited spill-over distance thus strongly reduces the catalytic effect of the large current collector stripes to our Pt nanoparticles. Future systematic variations of the Pt morphology experiments may reveal the width of the active region and thus the spill-over distance of oxygen on MIECs.

Finally, we want to emphasize again that the beneficial effect of Pt loading is particularly pronounced in low oxygen partial pressures, due to the opposite reaction orders of Pt-free and Pt loaded LSF64 surfaces. Accordingly, the question whether or not Pt (or any other metal) decoration improves the effective oxygen reduction kinetics in air depends on the interplay between catalytic state of the LSF64 electrode, size, shape and surface coverage of the metal particles and morphology of the entire mixed conducting electrode. The apparently contradicting results of measurements in literature, with often opposite or unclear outcome (see Introduction), may thus simply be caused by slight differences in these factors. Measurements at low pO_2 might have revealed a much clearer situation.

Conclusions

In this study we showed that decoration of $La_{0.6}Sr_{0.4}FeO_{3-\delta}$ (LSF64) thin film electrode surfaces with platinum nanoparticles (ca. 20 nm–40 nm diameter, ca. 4 nm–6 nm height, ca. 30% surface coverage) strongly lowers the polarization resistance of the electrode. At lower oxygen partial pressure (0.25 mbar) almost two orders of magnitude faster oxygen reduction kinetics was measured for Pt decorated films. Moreover, the Pt decorated surfaces exhibit an a very unusual pO_2 dependence of the polarization resistance, where less oxygen leads to lower polarization resistance (=faster reaction kinetics). Also the reproducibility of electrochemical properties and degradation behavior were improved by Pt decoration. All this can be explained by assuming a job splitting mechanism with Pt dissociating oxygen, spill-over of dissociated oxygen from Pt onto LSF64 and final ionization and incorporation into oxygen vacancies on the LSF64 surface. While without Pt oxygen dissociation on LSF64 is rate-limiting, Pt by-passes this slow step and rate-limiting oxygen ionization and incorporation on LSF64 remains.The negative reaction order with respect to oxygen is thus caused by the pO_2 dependency of the oxygen vacany concentration in LSF64.

Acknowledgments

Scanning electron microscopy was carried out by E. Eitenberger using facilities at the University Service Centre for Transmission Electron Microscopy (USTEM), TU Wien, Austria. The authors thank Austrian Sciene Fund (FWF) (project number: P31165—N37) for financial support. We also thank Huber Scientific for providing measurement equipment and W. Artner (X-Ray center, TU Wien) for his support in carrying out the XRD measurements.

ORCID

Christoph Riedl https://orcid.org/0000-0002-0739-8221
Johannes Bernardi https://orcid.org/0000-0002-4626-9246
Alexander Optiz https://orcid.org/0000-0002-2567-1885

References

1. E. Ivers-Tiffee, A. Weber, and D. Herbstritt, *J. Eur. Ceram. Soc.*, **21**, 1805 (2001).
2. B. A. Boukamp, *Nat. Mater.*, **2**, 294 (2003).
3. E. D. Wachsman and K. T. Lee, *Science*, **334**, 935 (2011).
4. Z. Gao, L. V. Mogni, E. C. Miller, J. G. Railsback, and S. A. Barnett, *Energy & Environmental Science*, **9**, 1602 (2016).
5. A. Nenning, L. Volgger, E. Miller, L. V. Mogni, S. Barnett, and J. Fleig, *J. Electrochem. Soc.*, **164**, F364 (2017).
6. W. Jung and H. L. Tuller, *Solid State Ionics*, **180**, 843 (2009).
7. A. Schmid, G. M. Rupp, and J. Fleig, *Phys. Chem. Chem. Phys.*, **20**, 12016 (2018).
8. S. Kogler, A. Nenning, G. M. Rupp, A. K. Opitz, and J. Fleig, *J. Electrochem. Soc.*, **162**, F317 (2015).
9. M. Søgaard, A. Bieberle-Hütter, P. V. Hendriksen, M. Mogensen, and H. L. Tuller, *Journal of Electroceramics*, **27**, 134 (2011).
10. A. K. Opitz, A. Nenning, C. Rameshan, R. Rameshan, R. Blume, M. Hävecker, A. Knop-Gericke, G. Rupprechter, J. Fleig, and B. Kloetzer, *Angew. Chem. Int. Ed.*, **54**, 2628 (2014).
11. F. S. Baumann, J. Fleig, H. U. Habermeier, and J. Maier, *Solid State Ionics*, **177**, 1071 (2006).
12. E. Bucher, W. Sitte, F. Klauser, and E. Bertel, *Solid State Ionics*, **191**, 61 (2011).
13. F. S. Baumann, J. Fleig, H. U. Habermeier, and J. Maier, *Solid State Ionics*, **177**, 3187 (2006).
14. B. Liu, Y. Zhang, and L. Zhang, *International Journal of Hydrogen Energy*, **34**, 1008 (2009).
15. G. M. Rupp, H. Tellez, J. Druce, A. Limbeck, T. Ishihara, J. Kilner, and J. Fleig, *J. Mater. Chem. A*, **3**, 22759 (2015).
16. G. M. Rupp, A. K. Opitz, A. Nenning, A. Limbeck, and J. Fleig, *Nat. Mater.*, **16**, 640 (2017).
17. G. M. Rupp, A. Limbeck, M. Kubicek, A. Penn, M. Stoger-Pollach, G. Friedbacher, and J. Fleig, *J. Mater. Chem. A*, **2**, 7099 (2014).
18. E. Bucher, W. Sitte, F. Klauser, and E. Bertel, *Solid State Ionics*, **208**, 43 (2012).
19. A. Egger, E. Bucher, M. Yang, and W. Sitte, *Solid State Ionics*, **225**, 55 (2012).
20. F. Pişkin, R. Bliem, and B. Yildiz, *Journal of Materials Chemistry A*, **6**, 14136 (2018).
21. J. Fleig, *Annu. Rev. Mater. Res.*, **33**, 361 (2003).
22. R. Merkle and J. Maier, *Phys. Chem. Chem. Phys.*, **4**, 4140 (2002).
23. N. Simrick, A. Bieberle-Hutter, T. Ryll, J. Kilner, A. Atkinson, and J. Rupp, *Solid State Ionics*, **206**, 7 (2012).
24. S. B. Adler, *Chem. Rev.*, **104**, 4791 (2004).
25. J. A. Kilner and M. Burriel, *Annu. Rev. Mater. Res.*, **44**, 365 (2014).
26. S. Skinner, *Solid State Ionics*, **135**, 709 (2000).
27. S. J. Skinner and J. A. Kilner, *Mater. Today*, **6**, 30 (2003).
28. W. Lee, J. W. Han, Y. Chen, Z. Cai, and B. Yildiz, *J. Am. Chem. Soc.*, **135**, 7909 (2013).
29. W. C. Chueh and S. M. Haile, *Annual Review of Chemical and Biomolecular Engineering*, **3**, 313 (2012).
30. A. Tarancon, S. J. Skinner, R. J. Chater, F. Hernández-Ramýorez, and J. A. Kilner, *Journal of Materials Chemistry*, **17**, 3175 (2007).
31. M. Rohnke, M. Falk, A.-K. Huber, and J. Janek, *Journal of Power Sources*, **221**, 97 (2013).
32. P. Plonczak, D. R. Sorensen, M. Sogaard, V. Esposito, and P. V. Hendriksen, *Solid State Ionics*, **217**, 54 (2012).
33. S.-L. Zhang, H. Wang, M. Y. Lu, C.-X. Li, C.-J. Li, and S. A. Barnett, *Journal of Power Sources*, **426**, 233 (2019).
34. W. C. Chueh and S. M. Haile, *Phys. Chem. Chem. Phys.*, **11**, 8144 (2009).
35. M. Kuhn, S. Hashimoto, K. Sato, K. Yashiro, and J. Mizusaki, *Solid State Ionics*, **195**, 7 (2011).
36. E. Bucher, C. Gspan, F. Hofer, and W. Sitte, *Solid State Ionics*, **238**, 15 (2013).
37. J. C. D. Vero, K. Develos-Bagarinao, S.-S. Liu, H. Kishimoto, T. Ishiyama, K. Yamaji, T. Horita, and H. Yokokawa, *J. Alloys Compd.*, **748**, 608 (2018).
38. E. Maguire, *Solid State Ionics*, **127**, 329 (2000).
39. E. Bucher and W. Sitte, *Solid State Ionics*, **192**, 480 (2011).
40. U. Lucia, *Renew. Sustain. Energy Rev.*, **30**, 164 (2014).
41. J. Wu and H. Yang, *Acc. Chem. Res.*, **46**, 1848 (2013).
42. Y. Takasu, N. Ohashi, X.-G. Zhang, Y. Murakami, H. Minagawa, S. Sato, and K. Yahikozawa, *Electrochimica Acta*, **41**, 2595 (1996).
43. B. Wang, *Journal of Power Sources*, **152**, 1 (2005).
44. A. M. Gomez-Marin and J. M. Feliu, *ChemSusChem*, **6**, 1091 (2013).
45. R. Usmen, E. Logothetis, and M. Shelef, *Sensors and Actuators B: Chemical*, **28**, 139 (1995).
46. A. K. Opitz and J. Fleig, *Solid State Ionics*, **181**, 684 (2010).
47. A. K. Opitz, A. Schintlmeister, H. Hutter, and J. Fleig, *Phys. Chem. Chem. Phys.*, **12**, 12734 (2010).
48. M. P. Hörlein, A. K. Opitz, and J. Fleig, *Solid State Ionics*, **247-248**, 56 (2013).
49. A. K. Opitz, M. P. Hörlein, T. Huber, and J. Fleig, *J. Electrochem. Soc.*, **159**, B502 (2012).
50. T. Huber, A. Opitz, and J. Fleig, *Solid State Ionics*, **273**, 8 (2015).
51. B. Luerßen, E. Mutoro, H. Fischer, S. Günther, R. Imbihl, and J. Janek, *Angew. Chem. Int. Ed.*, **45**, 1473 (2006).
52. G. Beck, H. Pöpke, B. Luerßen, and J. Janek, *J. Cryst. Growth*, **322**, 95 (2011).
53. G. Beck, H. Fischer, E. Mutoro, V. Srot, K. Petrikowski, E. Tchernychova, M. Wuttig, M. Ruhle, B. Luersen, and J. Janek, *Solid State Ionics*, **178**, 327 (2007).
54. E. Mutoro, B. Luerssen, S. Günther, and J. Janek, *Solid State Ionics*, **179**, 1214 (2008).

55. S. Heiroth, T. Lippert, A. Wokaun, M. Döbeli, J. Rupp, B. Scherrer, and L. Gauckler, *J. Eur. Ceram. Soc.*, **30**, 489 (2010).
56. A. Infortuna, A. Harvey, and L. Gauckler, *Adv. Funct. Mater.*, **18**, 127 (2007).
57. T. Ryll, H. Galinski, L. Schlagenhauf, P. Elser, J. L. M. Rupp, A. Bieberle-Hutter, and L. J. Gauckler, *Adv. Funct. Mater.*, **21**, 565 (2010).
58. J. L. Hertz, A. Rothschild, and H. L. Tuller, *Journal of Electroceramics*, **22**, 428 (2008).
59. J. Mizusaki, *Solid State Ionics*, **22**, 323 (1987).
60. Q. Fu, J. Yang, and Y. Luo, *The Journal of Physical Chemistry C*, **115**, 6864 (2011).
61. J. M. Bray and W. F. Schneider, *Langmuir*, **27**, 8177 (2011).
62. E. Navickas et al., *Phys. Chem. Chem. Phys.*, **17**, 7659 (2015).
63. H. Uchida, *J. Electrochem. Soc.*, **146**, 1 (1999).
64. J. Erning, T. Hauber, U. Stimming, and K. Wippermann, *Journal of Power Sources*, **61**, 205 (1996).
65. V. Haanappel, D. Rutenbeck, A. Mai, S. Uhlenbruck, D. Sebold, H. Wesemeyer, B. Röwekamp, C. Tropartz, and F. Tietz, *Journal of Power Sources*, **130**, 119 (2004).
66. J. M. Paige, Y. Cheng, P. A. Pepin, C. D. Curran, D. Sun, M. U. Chen, S. McIntosh, J. M. Vohs, and R. J. Gorte, *Solid State Ionics*, **341**, 115051 (2019).
67. Y. Cheng, A. S. Raman, J. Paige, L. Zhang, D. Sun, M. U. Chen, A. Vojvodic, R. J. Gorte, and J. M. Vohs, *The Journal of Physical Chemistry Letters*, **10**, 4082 (2019).
68. F. Bidrawn, G. Kim, N. Aramrueang, J. Vohs, and R. Gorte, *Journal of Power Sources*, **195**, 720 (2010).
69. T. Ryll, H. Galinski, L. Schlagenhauf, P. Elser, J. L. M. Rupp, A. Bieberle-Hutter, and L. J. Gauckler, *Adv. Funct. Mater.*, **21**, 565 (2010).
70. J. D. Rogers, V. S. Sundaram, G. G. Kleiman, S. G. C. Castro, R. A. Douglas, and A. C. Peterlevitz, *J. Phys. F*, **12**, 2097 (1982).
71. G. M. Bancroft, I. Adams, L. L. Coatsworth, C. D. Bennewitz, J. D. Brown, and W. D. Westwood, *Anal. Chem.*, **47**, 586 (1975).
72. M. Kubicek, G. M. Rupp, S. Huber, A. Penn, A. K. Opitz, J. Bernardi, M. Stöger-Pollach, H. Hutter, and J. Fleig, *Phys. Chem. Chem. Phys.*, **16**, 2715 (2014).
73. P. Hjalmarsson, M. Søgaard, and M. Mogensen, *Solid State Ionics*, **179**, 1422 (2008).
74. H. Wang and S. A. Barnett, *J. Electrochem. Soc.*, **165**, F564 (2018).
75. R. Kungas, A. S. Yu, J. Levine, J. M. Vohs, and R. J. Gorte, *J. Electrochem. Soc.*, **160**, F205 (2012).
76. J. Jamnik and J. Maier, *Phys. Chem. Chem. Phys.*, **3**, 1668 (2001).
77. G. J. Brug, A. L. van den Eeden, M. Sluyters-Rehbach, and J. H. Sluyters, *J. Electroanal. Chem.*, **176**, 275 (1984).
78. F. S. Baumann, J. Fleig, G. Cristiani, B. Stuhlhofer, H.-U. Habermeier, and J. Maier, *J. Electrochem. Soc.*, **154**, B931 (2007).
79. G. M. Rupp, A. Schmid, A. Nenning, and J. Fleig, *J. Electrochem. Soc.*, **163**, F564 (2016).
80. M. Escudero, A. Aguadero, J. Alonso, and L. Daza, *Journal of Electroanalytical Chemistry*, **611**, 107 (2007).
81. D. Chen, S. R. Bishop, and H. L. Tuller, *Journal of Electroceramics*, **28**, 62 (2012).
82. Z. Gao, X. Liu, B. Bergman, and Z. Zhao, *Journal of Power Sources*, **196**, 9195 (2011).
83. Y.-L. Huang, C. Pellegrinelli, and E. D. Wachsman, *ACS Catalysis*, **6**, 6025 (2016).
84. A. Schmid, G. M. Rupp, and J. Fleig, *Chemistry of Materials*, **30**, 4242 (2018).
85. A. Schmid and J. Fleig, *J. Electrochem. Soc.*, **166**, F831 (2019).
86. A. C. Luntz, M. D. Williams, and D. S. Bethune, *The Journal of Chemical Physics*, **89**, 4381 (1988).
87. C. T. Rettner and C. B. Mullins, *The Journal of Chemical Physics*, **94**, 1626 (1991).
88. L. Jacobse, A. den Dunnen, and L. B. F. Juurlink, *The Journal of Chemical Physics*, **143**, 014703 (2015).